Article:

Goodrich, J.P., Oechel, W.C., Gioli, B. et al. (4 more authors) (2016) Impact of different eddy covariance sensors, site set-up, and maintenance on the annual balance of CO2 and CH4 in the harsh Arctic environment. Agricultural and Forest Meteorology, 228-9. pp. 239-251. ISSN 0168-1923

https://doi.org/10.1016/j.agrformet.2016.07.008

Table 1. Sensor configurations and distances between analyzers at each site.

Sonic anemometers

Site	Model	Measurement height (m)	Orientation (°)	Heating configuration (dist. to Metek (cm))
CMDL	Gill WMP[a]	4.17	35	non-heated
BES	CSAT3[a]	2.18	60	non-heated
ATQ	CSAT3a	2.28	175	non-heated (35)
	Gill R3	2.28	0	non-heated (56)
	Metek	2.28	94	continuous
IVO	Metek[a]	3.42	205	intermittent

Gas analyzers

Site	Model	Measurement height (m)	Gas species	Intake tube length (m) (dist. to CP (cm))[b]	Dist. to primary anemometer (cm)
CMDL	LGR-FGGA-24EP	4.18	$CO_2/H_2O/CH_4$	5.71	18.00
	LI-7700	4.12	CH_4	(22.8)	23.10
BES	LI-7500	1.60	CO_2/H_2O	(36.5)	20.00
	LGR-FGGA-24EP	2.00	$CO_2/H_2O/CH_4$	4.50	16.50
ATQ	LI-7200	2.25	CO_2/H_2O	1.2	44.00
	LGR-FGGA-24EP	2.30	$CO_2/H_2O/CH_4$	3.12 (7.20)	43.00
IVO	LI-7200	3.22	CO_2/H_2O	1.2	14.00
	LI-7700	3.12	CH_4	-	45.00

[a]Primary anemometer used for flux calculation in gas analyzer comparisons.

[b]Distance to the closed or (en)closed-path (CP) analyzer used in comparisons.

Table 2. Data coverage for fluxes calculated with each sensor configuration. The continuously heated Metek is indicated by (con), the intermittently heated Metek is indicated by (int), closed- and (en)closed-path gas analyzers are indicated by (CP), and open-path analyzers are indicated by (OP).

Site	Flux	Sensor (pair)	% data remaining
ATQ	H	CSAT	53
	H	Metek (con)	62
	H	Gill R3	45
IVO	H	Metek (int)	59
BES	F_{CO2}	7500 (OP) - CSAT	25
	F_{CO2}	LGR (CP) - CSAT	44
ATQ	F_{CO2}	7200 (CP) - CSAT	43
	F_{CO2}	LGR (CP) - CSAT	46
	F_{CO2}	LGR (CP) - MTK (con)	52
BES	LE	7500 (OP) - CSAT	31
	LE	LGR (CP) - CSAT	49
ATQ	LE	7200 (CP) - CSAT	43
	LE	LGR (CP) - CSAT	52
	LE	LGR (CP) - MTK (con)	61
ATQ	F_{CH4}	LGR (CP) - CSAT	34
	F_{CH4}	LGR (CP) - MTK (con)	33
CMDL	F_{CH4}	7700 (OP) - Gill WP	26
	F_{CH4}	LGR (CP) - Gill WP	55
IVO	F_{CH4}	Metek (int)	42

Table 3. Comparison of summary statistics associated with spectral correction factors applied to fluxes at each site with different gas analyzers.

		Spectral correction factors		
Site	Flux & sensor	Median	1st quartile	3rd quartile
BES	F_{CO2} 7500	1.14	1.13	1.16
	F_{CO2} LGR	1.29	1.23	1.35
ATQ	F_{CO2} 7200	1.15	1.11	1.20
	F_{CO2} LGR	1.34	1.25	1.47
BES	LE 7500	1.14	1.13	1.15
	LE LGR	3.33	2.63	3.99
ATQ	LE 7200	2.34	1.99	2.89
	LE LGR	2.07	1.78	2.48
CMDL	F_{CH4} 7700	1.15	1.13	1.17
	F_{CH4} LGR	1.49	1.38	1.65

Table 4. Annual total F_{CO2} estimated with different sensor configurations at ATQ and BES.

Site	Gas analyzer	Anemometer	Annual F_{CO2} [gC m^{-2} yr^{-1}]
ATQ	LGR	CSAT	7.9 (± 1.3)
	LGR	Metek (heated)	7.5 (± 1.4)
	7200	CSAT	9.3 (± 1.1)
BES*	LGR	CSAT	-14.2 (± 1.7)
	7500	CSAT	-17.0 (± 1.1)

* Flux integrals for BES were calculated for 1 May to 31 October.

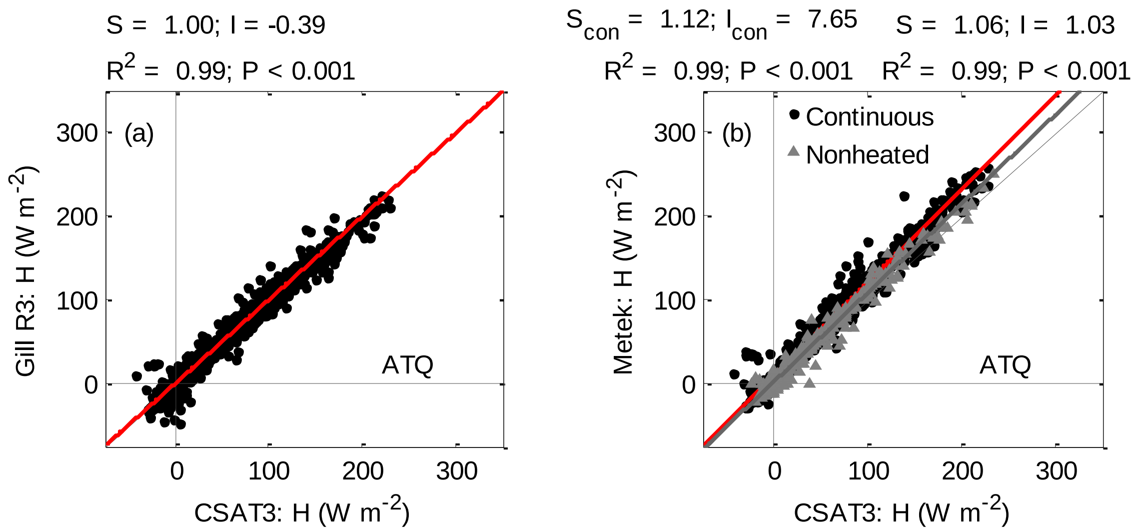

Figure 1. Comparisons of half-hourly sensible heat flux (H) at ATQ derived from the (unheated) CSAT3 anemometer and the (unheated) Gill R3 (*n* = 634) (a) and the heated Metek (*n* = 634) (b) from 1 October 2013 to 30 September 2014. The gray symbols in (b) represent data collected after heating of the Metek at ATQ was fully de-activated from 17 March to 11 June 2015 (*n* = 581). Regression coefficients with the 'con' subscript represent results from the continuously heated Metek data.

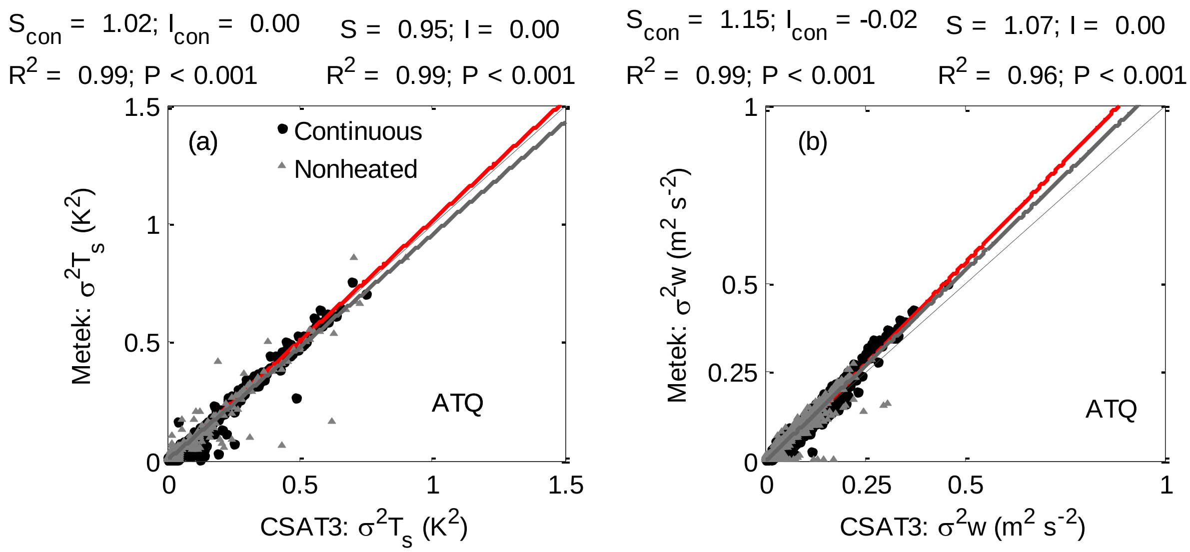

Figure 2. Comparisons of the CSAT3 and the heated Metek at ATQ of half-hourly variance in T_s (*n* = 634) (a) and *w* (*n* = 554) (b) from 1 October 2013 to 30 September 2014. The gray symbols represent data collected after heating of the Metek at ATQ was fully de-activated from 17 March to 11 June 2015 (*n* = 543). Regression coefficients with the 'con' subscript represent results from the continuously heated Metek data.

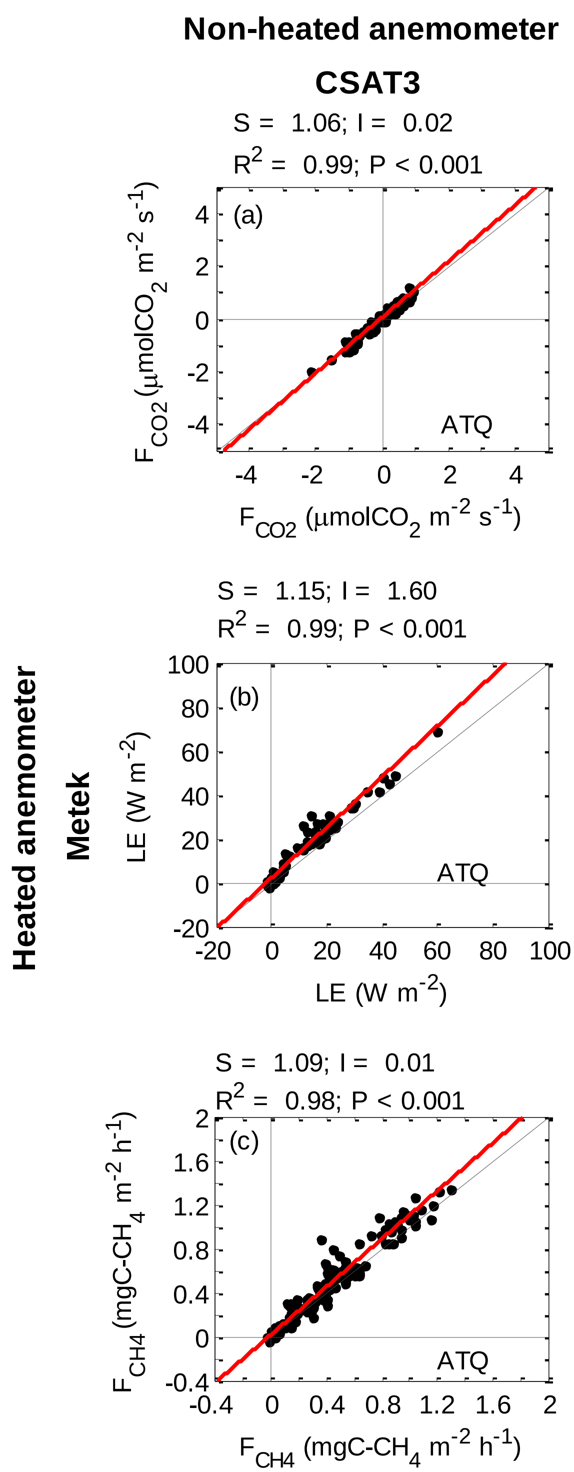

Figure 3. Comparison of daily mean CO_2 (n = 89) (a), LE (n = 81) (b), and CH_4 (n = 141) (c) fluxes derived from the heated Metek sonic anemometer (y-axis) and the non-heated CSAT3 anemometer, both paired with the LGR closed-path analyzer at ATQ. Half-hourly data were only used in daily mean calculations if both sensor pairs had good quality data (non-gaps).

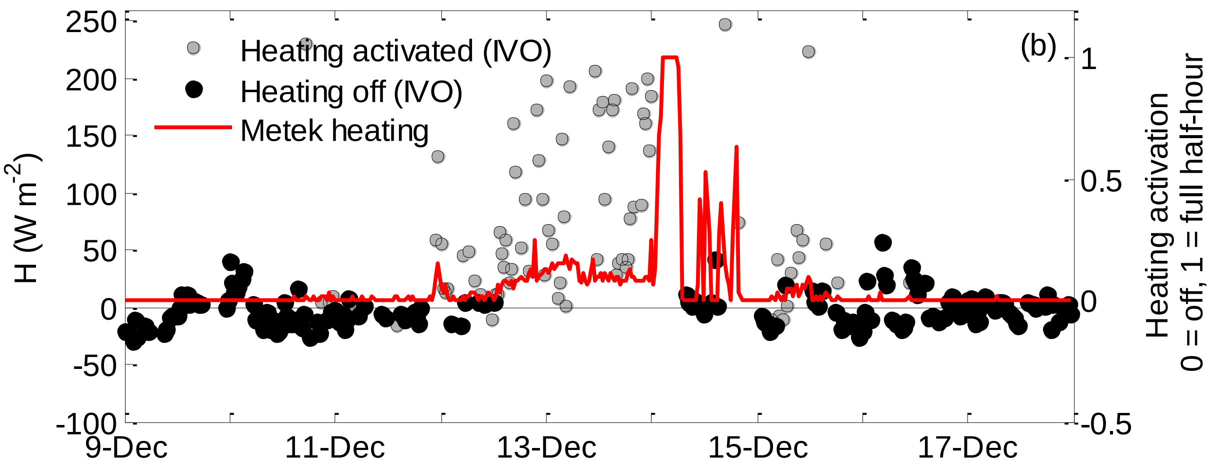

Figure 4. Sensible heat fluxes from IVO during a heating activation of the intermittently heated Metek anemometer. The solid red line shows the duration of heating. Grey points show noisy data resulting from the build-up of ice and snow and the resulting activation of anemometer heating.

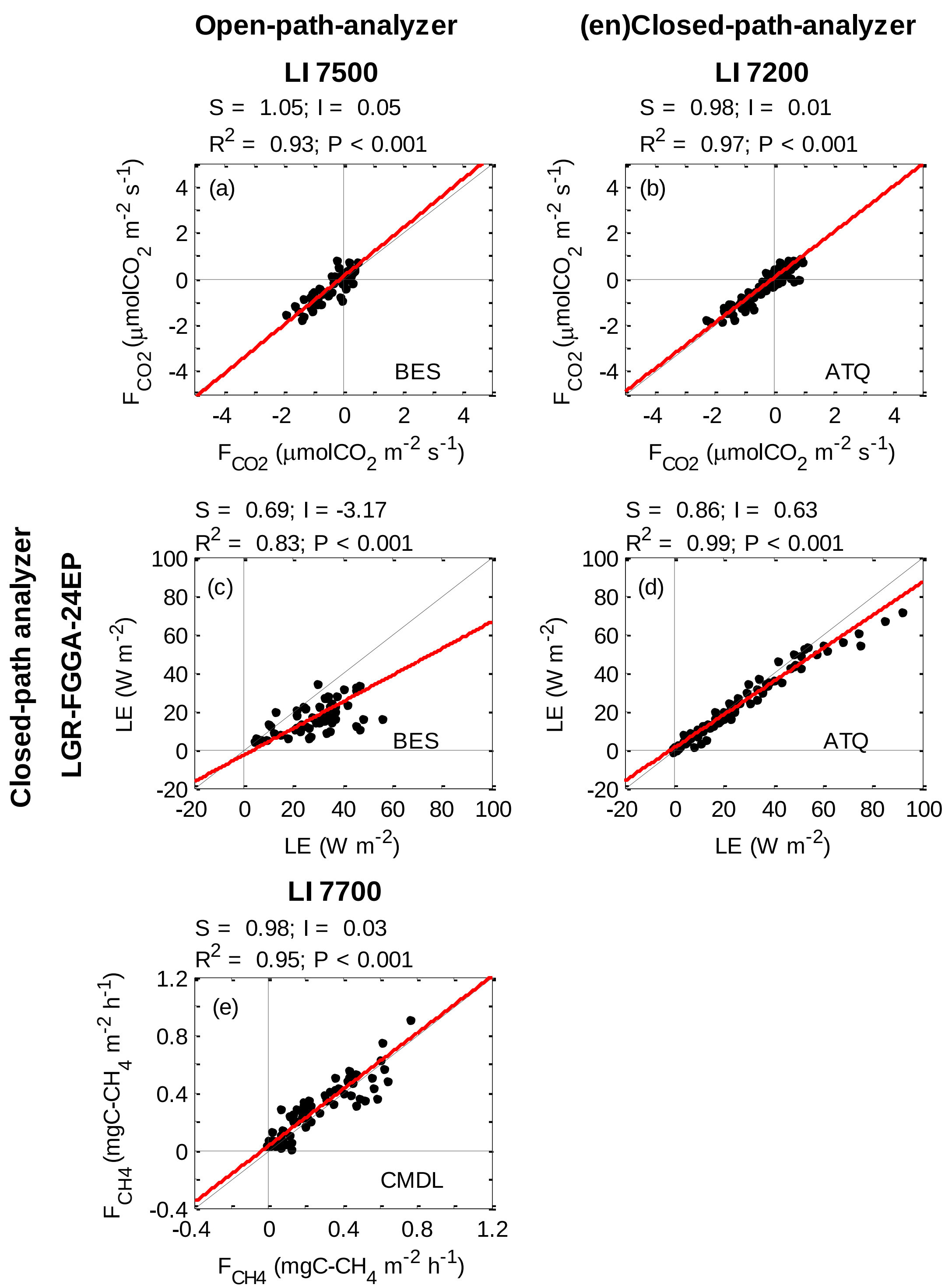

Figure 5. Comparisons of daily mean F_{CO2} (a), LE (c) and F_{CH4} (e) between open and closed-paths sensors at BES and CMDL, and comparisons of F_{CO2} (b) and LE (d) between closed and (en)closed-path sensors ATQ.

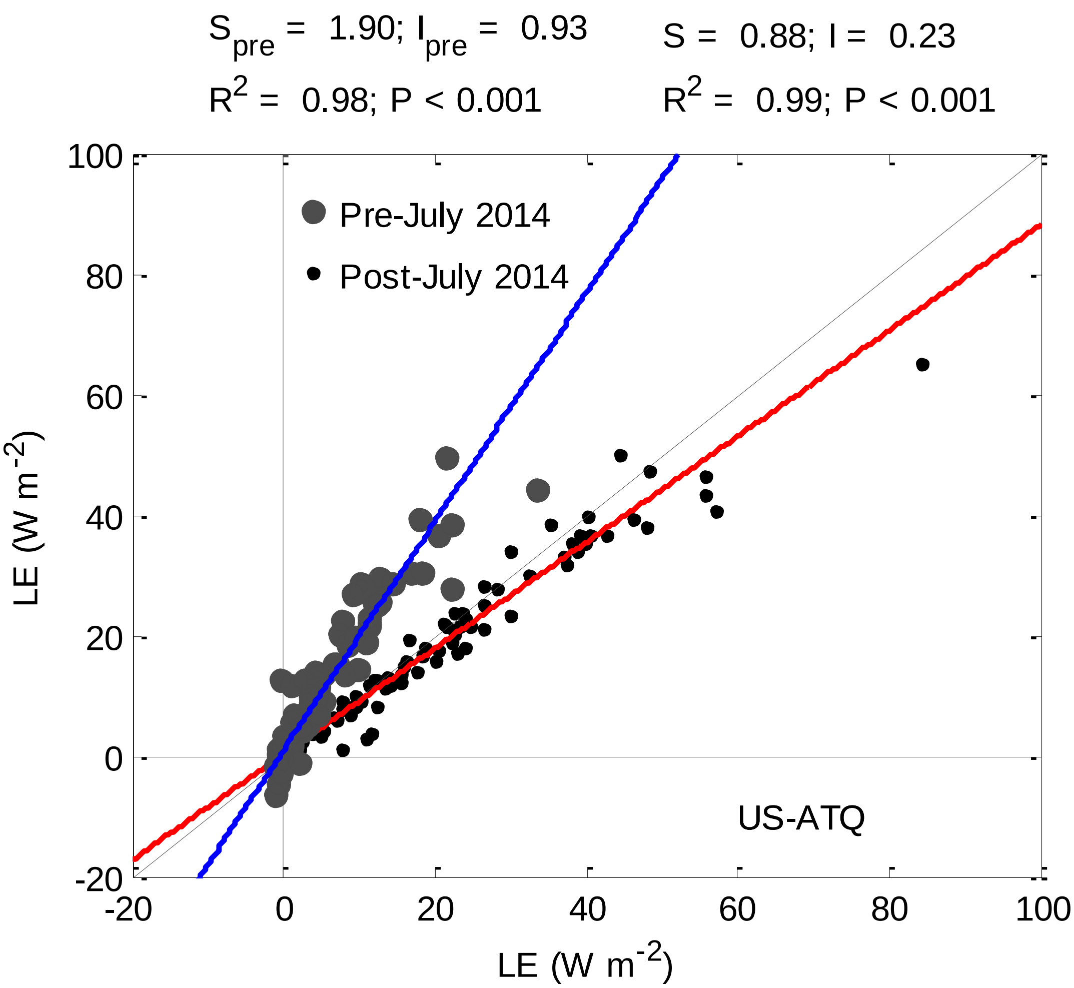

Figure S1. Comparisons of LE between closed and (en)closed-path sensors ATQ. The (en)closed-path LI-7200 was equipped with tube and rain cup of the larger pre-2013 design, which were subsequently replaced by smaller designs in mid-2014, greatly reducing attenuation of the H_2O signal and improving comparisons with the closed-path LGR-FGGA-24EP.

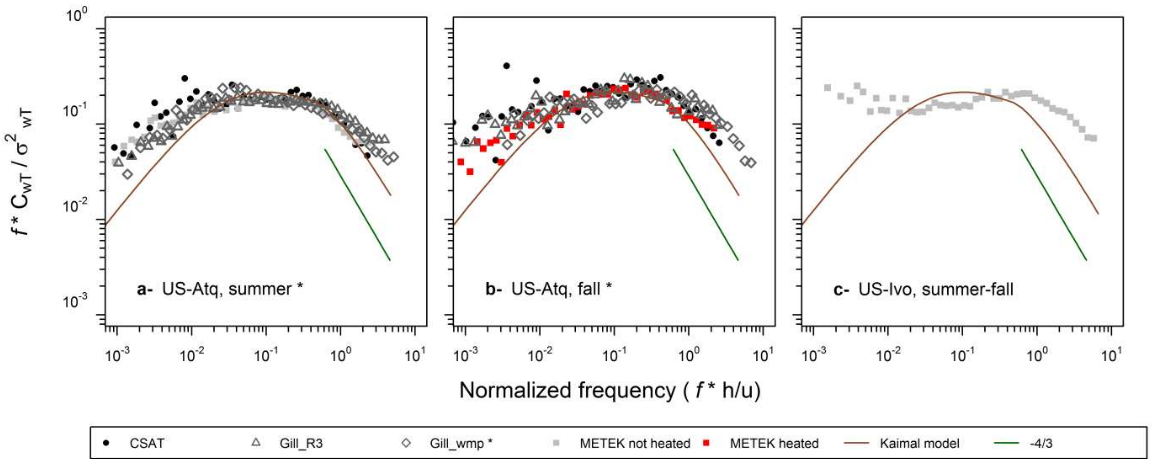

Figure S2. Daytime normalized binned-ensemble-averaged w'T' cospectra plotted versus normalized frequency for three sonic anemometers during periods when data from different anemometers were available at the same time: a. ATQ between the 15 August and the 27 August 2013, b. ATQ between 8 October and 31 October 2013, and c- IVO between the 8 October and 31 October 2013. Kaimal model for unstable and neutral conditions and-4/3 dampening slope are also shown for each site to provide a reference as to what should be expected for a high-frequency drop-off. * indicates that the Gill WMP used in CMDL has been added as for information purpose.

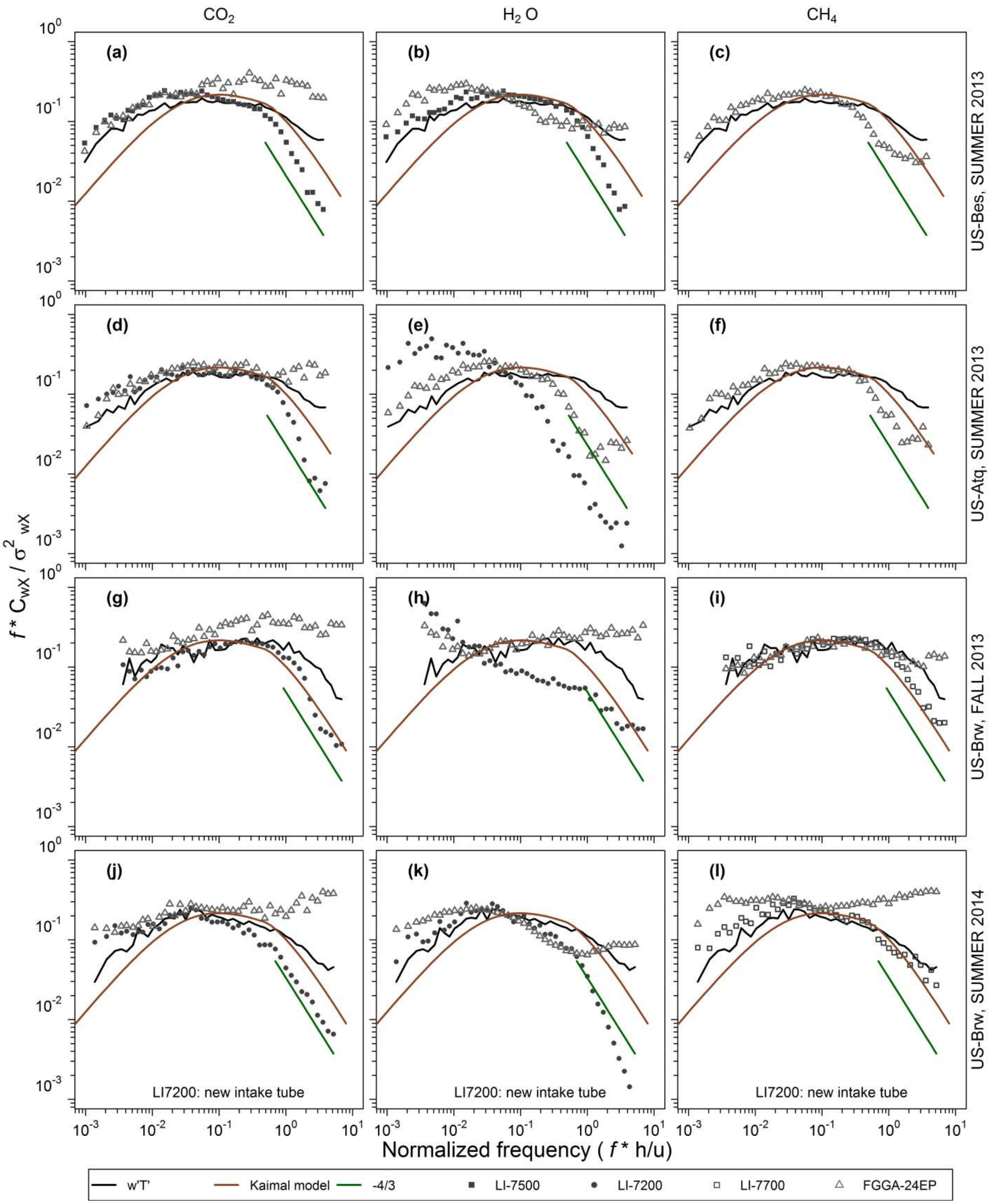

Figure S3. Daytime normalized binned-ensemble-averaged flux cospectra of CO_2 (a, d, g, j), H_2O (b, e, h, k) and CH_4 (c, f, i, l) plotted versus normalized frequency for three experimental sites during common periods when data from different measurements systems were available at the same time. Kaimal's model for unstable and neutral conditions and -4/3 slope are also shown for each site to provide a reference as to what should be expected for a high-frequency drop-off.